FTD-ID(RS)T-1063-90

FOREIGN TECHNOLOGY DIVISION

EXPERIMENTAL STUDIES OF LASER BEAM DEGRADATION BY TURBULENT SHEAR LAYERS

by

Yu Gang, Li Jiangguo, W.H. Christiansen

Approved for public release;
Distribution unlimited.

HUMAN TRANSLATION

FTD-ID(RS)T-1063-90 15 May 1991

MICROFICHE NR: FTD-91-C-000357

EXPERIMENTAL STUDIES OF LASER BEAM DEGRADATION BY TURBULENT SHEAR LAYERS

By: Yu Gang, Li Jiangguo, W.H. Christiansen

English pages: 14

Source: Zhongguo Jigung, Vol. 17, Nr. 4, 1990, pp. 198-204

Country of origin: China
Translated by: Leo Kanner Associates
F33657-88-D-2188
Requester: FTD/TTTD/Cason

PREPARED BY:

TRANSLATION DIVISION
FOREIGN TECHNOLOGY DIVISION
WPAFB OHIO

GRAPHICS DISCLAIMER

All figures, graphics, tables, equations, etc. merged into this translation were extracted from the best quality copy available.

EXPERIMENTAL STUDIES OF LASER BEAM DEGRADATION BY TURBULENT SHEAR LAYERS

Yu Gang and Li Jianguo, Institute of Mechanics, Chinese Academy of Sciences; W. H. Christiansen, University of Washington, Seattle, U.S.A.

Abstract: The degradation of a laser beam by turbulent shear layers has been systematically and experimentally studied with variation in parameters. The near-field measurement results showed that the growth rates of the shear layers decreased drastically with increase in Mach number and were dependent, to a lesser extent, on the density ratio. The optical far-field measurements results showed that the Strehl ratio decreased with increase in refractive index change across the shear layers, with increase in growth, with increase in downstream distance of the nozzle exit, and with increase in beam diameter.

Key words: turbulent shear layers, beam degradation.

I. Introduction

When a laser beam passes through a turbulent shear layer, inhomogeneity of the medium density in the layer will affect the focusing capability of the coherent light beam, thus degrading the quality of the far-field light beam. In the technical realm of high-energy lasers, sometimes a laser beam has to be outputted from an aperture from the surface of a high-speed moving object; for example, the turbulent flow mixed layer and tail wake in the cavity of a chemical laser, and the boundary surface of the

pneumatic window, and propagation problems [1 to 3] will be encountered in the turbulent flow medium of the light beam. Previous research neglected the function of the coherent large-scale eddy structure; however, these structures actually exist in some situations [4]. Moreover, theoretically the far-field graph of a light beam is the Fourier transform of the near-field graph because the near-field anomaly is the reason for the far-field light beam becoming degraded. The problem of light beam degradation has been studied over many years; however, there have been few simultaneous experimental analyses of near- and far-fields.

The near- and far-field light beam properties and their interrelationship with the laser beam passing through turbulent shear layers with a zero velocity ratio are the main topics of this experimental study. By drastically changing the density ratio and compressibility of the shear layers, the near-field data obtained with a M-Z interferometer and a schlieren camera were used in measuring the far-field graphs.

This paper was part of the work [5 to 7] of the authors while engaged at the Space Energy Laboratory, University of Washington, Seattle, United States.

II. Fundamental Relationship

The turbulent shear layers are the flow structure merged by two adjacent streams of gas flow with unequal velocities. The gas microclusters inside the flow structure not only can induce light scattering, but can also serve as a perturbation source of refractive index of the medium. Two characteristic lengths can be obtained here.

Thickness 1 of the shear layer: this is the percentage variation of the variation of a certain property (velocity,

temperature, or refractive index) of the gas flow relative to the free-stream value; and

the integrated turbulent flow scale Λ : when the velocity is not very high, the mean dimensions of the eddy are proportional to the shear layer thickness.

The relationship between the gasdynamic parameters and the optical properties can be represented as:

$$n=1+\beta\frac{\rho}{\rho_s} \tag{1}$$

In the equation, n is the refractive index of the gas, ρ_S is the reference density under standard conditions, and is the G-D constant. The phase change caused by the variation Δn of the refractive index in the turbulent shear layers is

$$\Delta\phi=\frac{2\pi}{\lambda}\int_0^L \Delta n ds \tag{2}$$

λ is wavelength, s is the optical path, and L is shear layer thickness.

Assume that the turbulent shear layers are isotropic; the light beam passes in the form of a plane wave. If the phase anomaly is a small quantity, then

$$I/I_0=\exp(-\langle\Delta\phi\rangle^2) \tag{3}$$

In the equation, $\langle\Delta\phi\rangle^2$ is the near-field phase root-mean-square error. I and I_0 are the light intensities at the far-field center for the light beam passing and not passing through the shear layers; the ratio is called the Strehl ratio, representing the extent of degradation of the light in the far field from the diffraction limit. Theoretically derived by Sutton [8], the root-mean-square phase difference is

$$\langle\Delta\phi\rangle^2=2k^2\langle\Delta n\rangle^2\Lambda L \tag{4}$$

In the equation, k is the wave number and $\langle\Delta n\rangle^2$ is the root-mean-square difference of the refractive index. When the gas flow velocity is not too high, $\langle\Delta\phi\rangle^2$ can be represented in a more convenient form [7]:

$$\langle\Delta\phi\rangle^2=0.5k^2\alpha^2\Delta n^2L^2 \tag{5}$$

In the equation, Δn is the difference of the refractive indexes of two sides of the shear layer, where α is a constant to be determined; when the gas flow is supersonic in velocity, consideration should be given to the effect of compressibility. In this case,

$$\langle \Delta\phi \rangle^2 = 2k^2 \Lambda L [\alpha^2 \Delta n^2 + (\bar{n}-1)\langle \Delta\rho \rangle^2 / \rho^2] \tag{6}$$

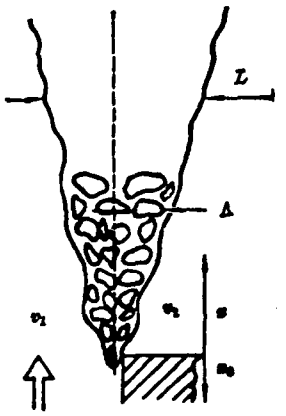

Fig. 1. Schematic diagram of turbulent shear layer

As actually observed, the near-field graph is the Airy disk, which is composed of a central bright spot and a series of concentric secondary-level bright rings. What was recorded in a photoelectric diode array is the integrated mean effect of the light intensity. The far-field peak value light intensity can be obtained by differentiating the power distribution P; P can be expressed as

$$P = \int_0^r \int_0^{2\pi} I(r, \theta) r \, dr \, d\theta \tag{7}$$

For circular shaped graphs, the differentiated form of the light intensity is

$$I = \frac{1}{2\pi r} d\left[\int_0^r 2\pi r I(r) dr\right] = \frac{1}{2\pi r} \frac{dP}{dr} \tag{8}$$

Then the Strehl ratio is

$$I/I_0 = \lim_{r \to 0} \left[\left(\frac{dP}{dr}\right) \Big/ \left(\frac{dP_0}{dr}\right)\right] \tag{9}$$

P and P_0 are the far-field powers of the light beam passing

through and not passing through the shear layer. Theoretically, the Strehl ratio is [9]

$$I/I_0 = (2J_1(x)/x)^2 \qquad (10)$$

In the equation, x=kaw, a is the light beam diameter, w is the value obtained by dividing the axial distance by the diametral coordinate on the image plane; $J_1(x)$ is the first-order Bessel function.

III. Experimental Arrangement

The authors designed and machined one subsonic nozzle and two supersonic nozzles (M=1.4, and 2.0). In the model design of the nozzle, the thickness of the exit boundary layer was reduced to the minimum; the exit cross section is 1.4cm x 1.4cm. From the nozzle exit, the gas jet enters the experimental section (1.4cm x 7.5cm x 7.5cm) with three faces of optical glass and one face communicating with the atmosphere. Then, at the opening side a planar shear layer is formed. At the nozzle exit, the atmospheric pressure is matched with the ambient pressure.

Among the experimental gases, there was SF_6, Ar, CO_2, He, and several types of gases with different blending ratios. At the cross section of the nozzle exit, the typical momentum thickness of the boundary layer is θ=0.0027mm (M = 0.1) and θ=0.058mm (M = 1.4). The range of variation in the Reynolds number is from $3.1 \cdot 10^4$ to $75 \cdot 10^4$. The following Mach numbers of the gas flow are involved: M=0.1, 0.6, 0.9, 1.4, and 2.0. For the density ratio, $\lambda_\rho = \rho_{Air}/\rho_{Gas}$, can range from 0.2 to 7.24.

The near-field phase data can be obtained with the M-Z interferometer, a shear interferometer, and a schlieren camera. When an He-Ne laser is used to obtain the time-averaged (10ms) data, a Q-tuned ruby laser was used to obtain the instantaneous data (100ns). The recording film, 3000ASA Polaroid, was used. By utilizing a He-Ne laser with filtration, beam extension,

alignment and grating, an experimental light beam with variable diameter approaching the diffraction limit was produced. The experimental light beam passed normally through the shear layer. To obtain the far-field graph on the optical platform, the condition $d>>a^2/\lambda$ should be satisfied; d is the far-field distance and a is the light beam diameter. Therefore, one beam contraction should be required for the light beam to pass through the shear layer.

The recording and data processing of the far-field graph was accomplished by using CCD (charge-coupled devices) 256x256 image elements of an EG&G Reticon camera, an image processor and a microcomputer. Within several seconds after each experiment, the time-averaged electronic image as well as the corresponding positions and light intensity information of the far-field graph can be obtained. By utilizing the custom software, the power distribution, the Strehl ratio, and other parameters can be displayed and printed out.

IV. Experimental Results

To explain the near-field measurement results, first three types of different pictures were observed. Fig. 2 (c) is the schlieren graph of the He-Air shear layer; the direction in which the photographs were taken parallelled the shear layer. Fig. 2 (b) is the interferogram of the CO_2/Air shear layer. Fig. 2 (a) is the interferogram of the SF_6/Air shear layer; the photography direction was normal to the shear layer. To obtain the quantitative results of light beam degradation in the far field, from Eq. (3), the main task of the near-field measurements was to obtain the data $<\Delta\phi>^2$, which can be obtained by changing the displacement of the interference streak as shown in Fig. 3. Apparently, for such a complex streak diagram, without a set of an advanced data read/write processing system, the work was time-consuming and imprecise. The authors tried to conduct manual

reading and write together with a computer, but the results are not satisfactory.

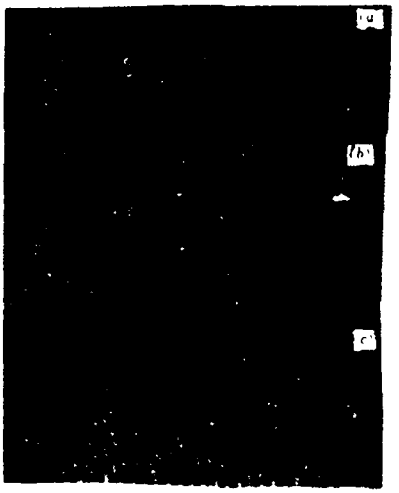

Fig. 2.
Remark: (c) Schlieren graph of He/Air shear layer. The He gas flow is at the bottom, M=1.4, from left to right; (b) Interferogram of CO_2/Air shear layer. The CO_2 gas flow is at the top, M=0.6, from left to right, with time exposure intervals of 40 ns; He-Ne laser light source; (a) SF_6/Air shear layer interferogram. SF_6 gas flow, M=0.1, from left to right, ruby laser source, pulse duration 100 ns

However, to obtain $\langle\Delta\phi\rangle^2$ the shear layer thickness should be known; this is the only length factor related to light beam degradation in the far field; this can be obtained from calculation of the time-averaged interferogram parallel to the shear layer as shown in Fig. 2 (b).

Because of the effect of fluctuations and noise, only the visible interferogram of $M \leq 0.1$ can be obtained with an M-Z interferometer. A difference interferometer is insensitive to fluctuations; an interferogram of M=0.6 can be obtained but the difficulty in data processing is increased. Fig. 3 is a

typical distribution curve of the refractive index obtained from calculation of an M-Z interferogram. Obtained from three

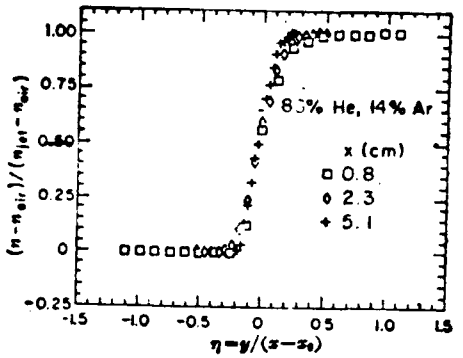

Fig. 3. Distribution curve of dimensionless refractive index
Remark: η is the dimensionless lateral-direction coordinate, x_0 is the position of the virtual origin of coordinates; the various symbols represent the downstream positions

different downstream cross sections, the refractive index distribution is nearly entirely coincident; this explains the good self-modeling. The expansion rate of the shear layer is defined such that the relative variation in the refractive index on the connecting curve is the slope of the straight line connecting two points 0.1 and 0.9.

The schlieren graph, Fig. 2 (c), can more directly display the expansion situation of the shear layer. From the expansion situation, the thickness δ_{vis} of the shear layer can be measured. This can be done only by measuring the included angle between two straight lines [4] tangent to the edge of the shear layer. Considering the imprecision of the definition of an edge, a 10 to 20% error is possible.

Two primary factors that affect the thickness of the shear layer include the density ratio λ_ρ and the compressibility, the M number. Fig. 4 (a) includes nine types of gases and six M numbers. From the figure, the shear layer thickness increases

with increase in the density ratio, and decreases with increase in M. As indicated in Fig. 4 (b), the regional variation in the shear layer thickness nearing M=1 is much faster than in other regions; such as, from M=0.1 to M=2.0, the shear layer thickness increases by a factor of 2.5 to 3.5. However, notwithstanding that the density ratio increases by 36 times from 0.2 to 7.2, the shear layer thickness changes by only 30%.

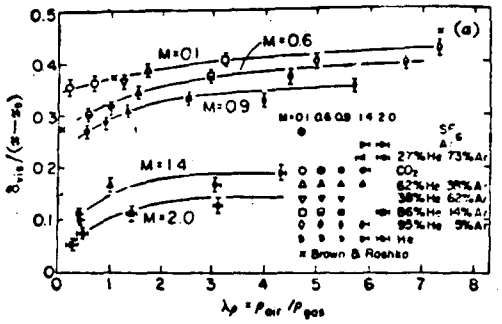

Fig. 4(a). Variation curves showing that the shear layer expansion rate varies with density ratio

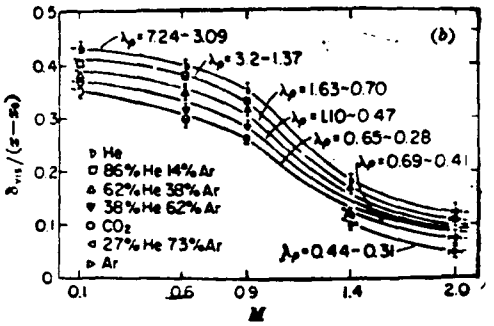

Fig. 4(b). Variation curves showing that the shear layer expansion rate varies with the M number

Fig. 5 is a group of far-field graphs for a set of light beams of 0.5cm and 1.0cm passing through three different shear layers at 1cm downstream from the nozzle exit; the corresponding schlieren graphs of the shear layers are on the lower side. Apparently, the degradation effect on the light beam is the smallest for the density-matched shear layers with 38% He and 62% Ar/Air (λ_ρ=1.1). The degradation is serious in a situation with density mismatching; however, there are different degrees of scattering in the horizontal direction. This means that there is possibly a structure similar to a grating function in the shear layer.

Fig. 6 shows records made with the CCD camera: for the simulated three-dimensional far-field graphs from computer graphics, the light beam diameter is 0.5cm; the measuring point

is located at 2cm downstream from the nozzle exit. The light exposure time is 0.1s.

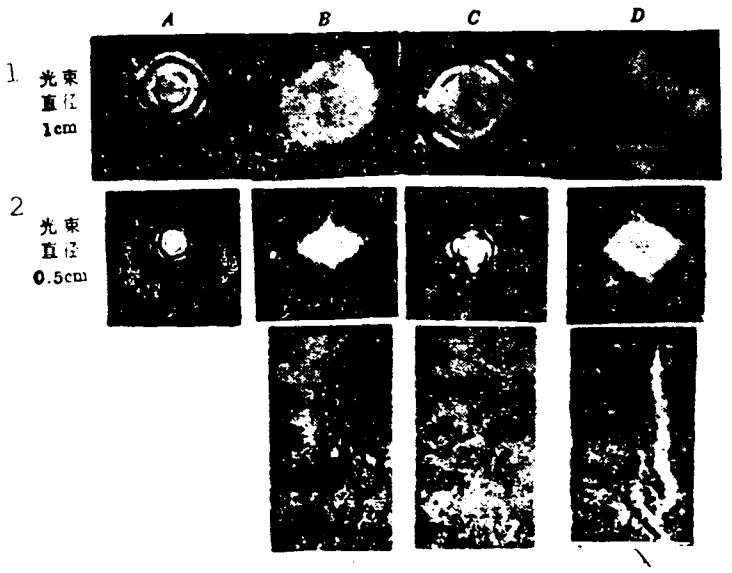

Fig. 5. Far-field graphs for light beam passing through different shear layers
Remark: A - Reference light beam B - Passing through shear layer with 62% He and 38% Ar/Air C - Passing through shear layer with 38% He and 62% Ar/Air D - Passing through shear layer of SF_6/Air
KEY: 1 - 1cm diameter light beam 2 - 0.5cm diameter light beam

As discovered from data similar to that in Fig. 7, the diameter of the constricting light beam can significantly raise the Strehl ratio. For the case of a shear layer M=0.6 with 86% He and 14% Ar/Air, when the light beam diameter constricts from 1cm to 0.5cm, the Strehl ratio is increased by 27%; the purpose of constricting the light beam is to reduce D/Λ.

When the downstream distance is increased, the decrease in the Strehl ratio is very significant. For example, the shear

layer for a light beam diameter of 0.5cm with 86% He and 14%Ar/Air shifts the light beam from a location 1cm from the

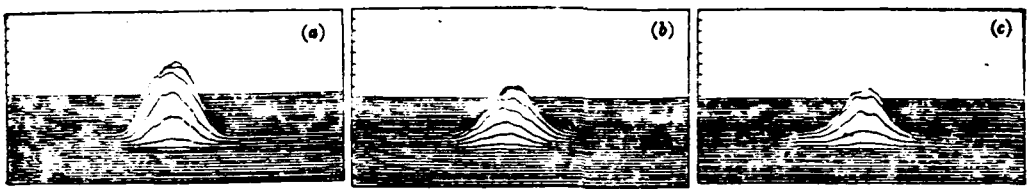

Fig. 6. Quasi-three-dimensional far-field graphs
Remark: (a) Light beam not passing through a shear layer (b) Light beam passing through a shear layer with M=0.6 with 62% He and 38% Ar/Air (c) Light beam passing through a shear layer M=1.4 with 62% He 38% Ar/Air

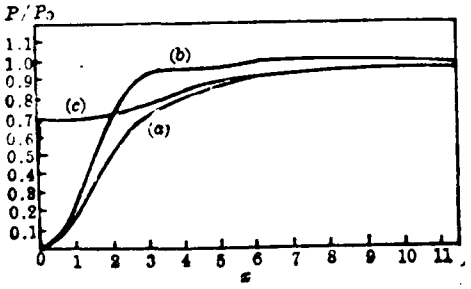

Fig. 7. Power distribution curve
Remark: (a) Corresponding to Fig. 6 (b); (b) Corresponding to Fig. 6 (a); (c) Ratio of (a) and (b), representing the Strehl ratio

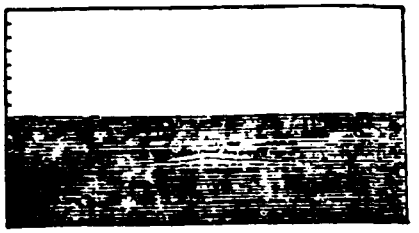

Fig. 8. Quasi-three-dimensional far-field graph
Remark: Light beam passing through shear layer M=0.01 with He/Air

nozzle exit to the location 2cm, the Strehl ratio can be reduced by 50%.

An increase in the density ratio will thicken the shear layer, thus causing a decrease in the Strehl ratio.

A variation in the Mach number M will induce a corresponding change Δn, λ_ρ, and L. At low M numbers, large-scale eddy ordered structure will appear in the shear layer, thus causing a severe degradation of the light beam quality. Fig. 8 shows a far-field graph almost degraded because of a factor not yet fully clarified, possibly due to the effect of the sequential structure in the layer. The refractive surface formed by these structures caused irregular refraction of the light beam, thus causing severe phase anomalies. At high M numbers, the Strehl ratio can be improved.

From Eq. (5), if the constant to be determined is known, thus the very time-consuming calculation of the symbol $\langle\Delta n\rangle^2$ is not required; this is a very considerable simplification in estimating the far-field degradation of the light beam. To obtain the value α, the near-field measured L value and the far-field Strehl ratio (simplified as SR) to be considered as the $SR\sim(\Delta n\cdot L)^2$ relationship diagram for obtaining the value α. Figs. 9 (a) and (b) are two sets of typical results with the light beam diameter of 0.5cm, M=0.9, and at the 1cm and at the 2cm locations downstream from the nozzle exit. By coincidence with a straight line, the value α can be obtained by using the slope rate; the value of α should be a constant with a value approximately consistent with the value given in [3]. The authors attempted to obtain the value α for the light beam diameter of 1cm; however, no straight line could be obtained. So further study is required. Whether a large diameter light beam is always more easily affected.

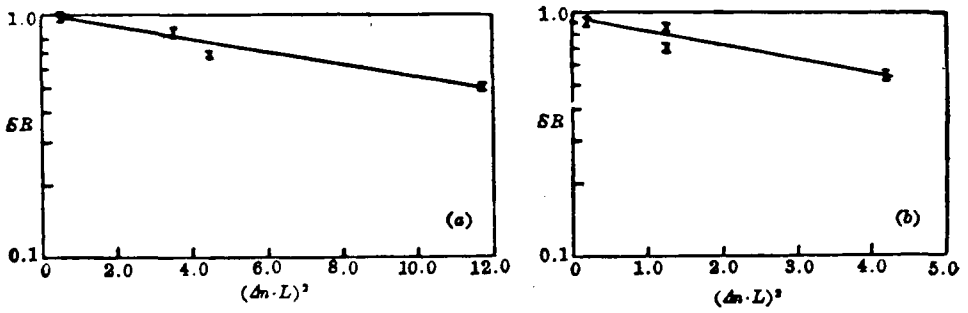

Fig. 9. Relationship diagram of SR~$(\Delta n \cdot L)^2$
Remark: For a light beam diameter of 0.5cm, (a), M=0.9, and (b), M=0.1

V. Conclusions

As indicated by the experimental results, light beam quality is degraded in the far field, the degradation worsens with increase in the refractive index on both sides of the shear layer, the degradation increase with increase in thickness of the shear layer, the degradation increases with increase in downstream distance, and degradation increases with increase in light beam diameter.

Cai Yongpei and C. B. Thomas also took part in the research on this subject.

The paper was received on 29 February 1988.

REFERENCES

1. Christiansen, W. H. et al., Rev. Fluid Mech. 7, 115 (1975).
2. Legner, H. H. et al, "Laser beam degradation through turbulent interface," AIAA Paper, 78-71 (1980).
3. Vu, B. T. et al, "Laser beam degradation through optically turbulent mixing layers," AIAA Paper, 80-1414 (1980).

4. Brown, G. L. and A. Roshko, J. Fluid Mechanics 46, 175 (1974).
5. Christiansen, W. H. et al, "A study of inhomogeneous shear layers and their effect on laser beam degradation," 5th GCL Symposium, Oxford, August 10-24 (1984).
6. Johari, H. et al, "A preliminary study of inhomogeneous shear layers," AIAA Paper, 84-1621 (1984).
7. Christiansen, W. H. and G. Yu, "Optics of inhomogeneous shear layers," International Fluid Conference, Beijing, July (1987).
8. Sutton, G. W., "Effect of turbulent fluctuations in an optically active fluid medium," AIAA J. 7/9, 1737 (1969).
9. Born, M. and E. Wolf, Principles of Optics, Pergamon Press, Oxford, 1964.

DISTRIBUTION LIST

DISTRIBUTION DIRECT TO RECIPIENT

ORGANIZATION	MICROFICHE
B085 DIA/RTS-2FI	1
C509 BALLOC509 BALLISTIC RES LAB	1
C510 R&T LABS/AVEADCOM	1
C513 ARRADCOM	1
C535 AVRADCOM/TSARCOM	1
C539 TRASANA	1
Q591 FSTC	4
Q619 MSIC REDSTONE	1
Q008 NTIC	1
Q043 AFMIC-IS	1
E051 HQ USAF/INET	1
E404 AEDC/DOF	1
E408 AFWL	1
E410 AD/IND	1
E411 ASD/FTD/TTIA	1
F429 SD/IND	1
P005 DOE/ISA/DDI	1
P050 CIA/OCR/ADD/SD	2
R085 NASA/NST-44	1
AFIT/LDE	1
CCV	1
NASA/NST-44	1
NSA/P090/CDB	2
FSL	1